The status of the Excited Baryon Analysis Center

B. Juliá-Díaz

Department d'Estructura i Constituents de la Matèria and Institut de Ciències del Cosmos, Universitat de Barcelona, E–08028 Barcelona, Spain

Abstract. The Excited Baryon Analysis Center (EBAC), which is associated with the Theory Group at Jefferson Laboratory, was initiated in 2006. Its main goal is to extract and interpret properties of nucleon resonances (N*) from the world data of meson production reactions induced by pions, photons and electrons. We review the main accomplishments of the center since then and sketch its near future perspectives.

Keywords: Nucleon Resonances, photoproduction, electroproduction
PACS: 14.20.Gk, 13.75.Gx, 13.60.Le

The spectrum of low-lying nucleon and Δ resonances is a primordial ingredient for any understanding of the non-perturbative domain of strong interactions. Consequently, a large effort has been made during the last years to extract properties of N^* from the world data base of $\pi N \to \pi N$ and $\gamma(^*)N \to \pi N$ data [1]. The most relevant recent advances in our knowledge of N^* physics are due to the effort carried out mostly in facilities like Jefferson Lab (USA) or MAMI and CB-ELSA (Germany) where the probe used is electromagnetic, thus permitting a cleaner access to the baryon structure.

The use of electromagnetic probes to explore the inner structure of baryons does not completely avoid the difficulties arising from the not so well-known hadronic pieces of the production process. Thus, it is well acknowledged that one needs to attain a proper understanding of the hadronic interactions entering in the electromagnetic production processes to be able to extract any useful information for their analysis. This is achieved by the construction of involved dynamical models which incorporate the main physics at stake, e.g. most relevant channels, unitarity, and which can correlate the vast amount of data existing for both single and double meson production reactions.

Among the existing theoretical approaches, the one taken at the Excited Baryon Analysis Center (EBAC) tries to encompass the above by considering the following two and three body channels: γN, πN, $\pi\pi N$, ηN in a multi-channels multi-resonances framework [2]. The starting point of the model is a set of Lagrangians describing the interactions between mesons (including the photon) ($M = \gamma,\ \pi, \eta\ ,\ \rho, \omega,\ \sigma, \ldots$) and baryons ($B = N, \Delta, N^*, \ldots$). By applying a unitary transformation method [3], an effective Hamiltonian, with an energy independent set of potentials, is then derived from the considered Lagrangian.

The meson-baryon (MB) scattering amplitudes are obtained in the following way,

$$T_{\alpha,\beta}(E) \quad = \quad t_{\alpha,\beta}(E) + t^R_{\alpha,\beta}(E)\,, \tag{1}$$

where $\alpha, \beta = \gamma N, \pi N, \eta N, \pi\pi N$. The full amplitudes, e.g. $T_{\pi N,\pi N}(E)$, $T_{\eta N,\pi N}(E)$, $T_{\pi N,\gamma N}(E)$ can be directly used to, within the same framework, compute $\pi N \to \pi N, \eta N$ and $\gamma N \to \pi N$, $\gamma N \to \eta N$, scattering observables. The non-resonant amplitude $t_{\alpha,\beta}(E)$ in Eq. (1) is defined by the coupled-channels equations,

$$t_{\alpha,\beta}(E) = V_{\alpha,\beta}(E) + \sum_{\delta} V_{\alpha,\delta}(E)\, G_\delta(E)\, t_{\delta,\beta}(E) \tag{2}$$

with $V_{\alpha,\beta}(E) = v_{\alpha,\beta} + Z^{(E)}_{\alpha,\beta}$, where $v_{\alpha,\beta}$ are the non-resonant MB potentials and $Z^{(E)}_{\alpha,\beta}$ is due to the one-particle-exchange between unstable $\pi\Delta, \rho N, \sigma N$ states which are the resonant components of the $\pi\pi N$ channel.

The second term in the right-hand-side of Eq. (1) is the resonant term defined by

$$t^R_{\alpha,\beta}(E) = \sum_{N^*_i, N^*_j} \bar{\Gamma}_{\alpha\to N^*_i}(E)[D(E)]_{i,j}\bar{\Gamma}_{N^*_j\to\beta}(E)\,, \tag{3}$$

with

$$[D^{-1}(E)]_{i,j} = (E - M^0_{N^*_i})\delta_{i,j} - \sum_{\delta} \Gamma_{N^*_i\to\delta} G_\delta(E) \bar{\Gamma}_{\delta\to N^*_j}(E)\,. \tag{4}$$

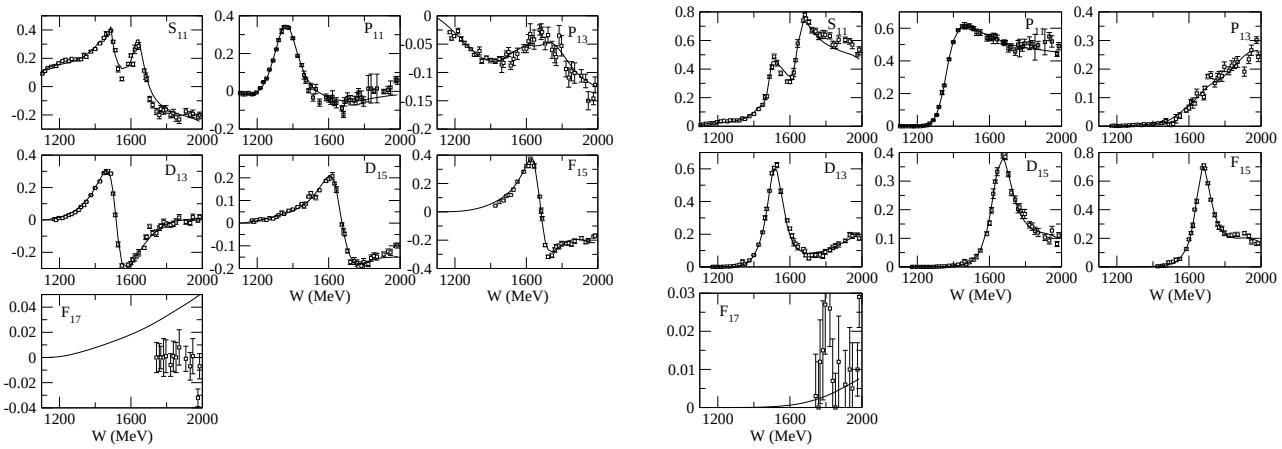

FIGURE 1. Real (left) and imaginary (right) parts of the calculated πN partial wave amplitudes (Eq. (1)) of isospin $T = 1/2$ are compared with the energy independent solutions of Ref. [4].

where $M^0_{N^*}$ is the bare mass of the resonant state N^*. The dressed vertex interactions in Eq. (3) and Eq. (4) are (defining $\Gamma_{\alpha\to N^*} = \Gamma^\dagger_{N^*\to\alpha}$)

$$\bar{\Gamma}_{\alpha\to N^*}(E) = \Gamma_{\alpha\to N^*} + \sum_\delta t_{\alpha,\delta}(E) G_\delta(E) \Gamma_{\delta\to N^*}\,, \tag{5}$$

$$\bar{\Gamma}_{N^*\to\alpha}(E) = \Gamma_{N^*\to\alpha} + \sum_\delta \Gamma_{N^*\to\delta} G_\delta(E) t_{\delta,\alpha}(E)\,. \tag{6}$$

DEVELOPMENTS IN HADRONIC REACTIONS

Within the framework sketched above we built a hadronic model, JLMS, which was aimed at properly describing the $\pi N \to \pi N$ and $\pi N \to \eta N$ experimental data in the energy range relevant for N^* physics, 1 GeV $< W_{\rm c.m.} <$ 2 GeV [5]. The model was built by performing extensive χ^2 minimizations to the experimental data collected from the GWU-SAID database [4] and to the partial wave amplitudes of the GWU-SAID group. In fig. 1 the real and imaginary part of the scattering amplitudes for $\pi N \to \pi N$ reactions are compared to the GWU-SAID ones for several partial waves. The agreement is in most waves extremely good, with the only exception of the S_{31} partial wave, which does not agree with the same quality.

The $\pi N \to \pi N$ model predictions are given in detail in Ref. [5], with explicit comparisons to experimental data both for differential cross sections and polarizations as well as for the total cross sections predicted by the model.

N^* properties from the analytic continuation of the scattering amplitudes

Extracting the properties, e.g. masses, widths, and couplings to MB channels, of the resonances from a hadronic model is in general not an easy task. A proper extension of the model to the complex energy plane is needed so that poles of the $t-$matrix can be isolated and their properties extracted. The analytic extension of the dynamical coupled-channels model described above has been done in Refs. [6, 7]. In table 1 we provide the position in the complex$-E$ plane of all the poles present in our πN model [8]. First, let us note that most of the pole positions agree within errors with those already reported by the PDG [9]. However, similarly to the recent developments from the GWU-SAID group [4], our model does not find any poles corresponding to several of the N^* states present in the PDG and rated with three or less stars. Also, we do not find poles in the P_{13} and P_{31} partial waves.

TABLE 1. The resonance pole positions M_R [listed as $(\mathrm{Re}\, M_R, -\mathrm{Im}\, M_R)$] extracted from the JLMS model in the different unphysical sheets are compared with the values of 3- and 4-stars nucleon resonances listed in the PDG [9]. The notation indicating their locations on the Riemann surface are explained in the text. "—" for $P_{33}(1600)$, P_{13} and P_{31} indicates that no resonance pole has been found in the considered complex energy region, $\mathrm{Re}(E) \leq 2000$ MeV and $-\mathrm{Im}(E) \leq 250$ MeV. All masses are in MeV.

	$M^0_{N^*}$	M_R	Location	PDG
S_{11}	1800	(1540, 191)	$(uuuupp)$	(1490 - 1530, 45 - 125)
	1880	(1642, 41)	$(uuuupp)$	(1640 - 1670, 75 - 90)
P_{11}	1763	(1357, 76)	$(upuupp)$	(1350 - 1380, 80 - 110)
	1763	(1364, 105)	$(upuppp)$	
	1763	(1820, 248)	$(uuuuup)$	(1670 - 1770, 40 - 190)
P_{13}	1711	—		(1660 - 1690, 57 - 138)
D_{13}	1899	(1521, 58)	$(uuuupp)$	(1505 - 1515, 52 - 60)
D_{15}	1898	(1654, 77)	$(uuuupp)$	(1655 - 1665, 62 - 75)
F_{15}	2187	(1674, 53)	$(uuuupp)$	(1665 - 1680, 55 - 68)
S_{31}	1850	(1563, 95)	$(u-uup-)$	(1590 - 1610, 57 - 60)
P_{31}	1900	—		(1830 - 1880, 100 - 250)
P_{33}	1391	(1211, 50)	$(u-ppp-)$	(1209 - 1211, 49 - 51)
	1600	—		(1500 - 1700, 200 - 400)
D_{33}	1976	(1604, 106)	$(u-uup-)$	(1620 - 1680, 80 - 120)
F_{35}	2162	(1738, 110)	$(u-uuu-)$	(1825 - 1835, 132 - 150)
	2162	(1928, 165)	$(u-uuu-)$	
F_{37}	2138	(1858, 100)	$(u-uuu-)$	(1870 - 1890, 110 - 130)

A new perspective on P_{11} nucleon resonances

As described in detail in Ref. [8] the determination of resonance poles in the P_{11} partial wave has been difficult since the discovery of the Roper resonance in 1964. In our model we find two poles near the PDG value $(\mathrm{Re}\, M_R, -\mathrm{Im}\, M_R) = (1350-1380,\ 80-110)$ corresponding to the Roper, $N^*(1440)$, resonance. This finding is consistent with the results from the analysis by Cutkosky and Wang [10] (CMB), GWU/VPI [4] and Jülich [11].

A higher mass pole at $(1820, 248)$ in the same partial wave, which is close to the $N^*(1710)$ state listed by PDG is also found. Moreover, within our model we find that this pole and the two corresponding the Roper resonance are related to only one bare state. This common bare state can be pictured by depicting the evolution of the pole positions as we vary the coupling to the different inelastic channels, see Fig. 2.

Analysis of the $\pi N \to \pi\pi N$ reactions

The production of two or more pions provides precious information on the way N^* couple to the higher meson-baryon channels. At moderately low center of mass energies, e.g. $W \sim 1500$ MeV, the importance of $\pi\pi N$ channels is already sizeable and therefore it is important not only to incorporate such channels into the framework but also to have experimental data to properly constrain their couplings. The analysis of the $\pi N \to \pi\pi N$ reaction provides a first test of such ingredients present in our model. This information would, in principle, be very useful to build the hadronic model. However, due to the lack of enough experimental data we could not profit from these data in our minimizations. The full details of our calculation are given in Ref. [12]. In figure 3 we provide a comparison of the predicted total cross sections compared to data. In the same figure we include the results obtained without the inclusion of the direct $2-3$ mechanisms.

An improved model for $\pi N \to \eta N$

The JLMS model was mostly constrained from the $\pi N \to \pi N$ data. Thus, it was expected that some of parameters related to the ηN channels were not well constrained. In Ref. [14] we considered the full $\pi N \to \eta N$ data-base and performed χ^2 minimizations to further constrain the parameters related to the ηN channel.

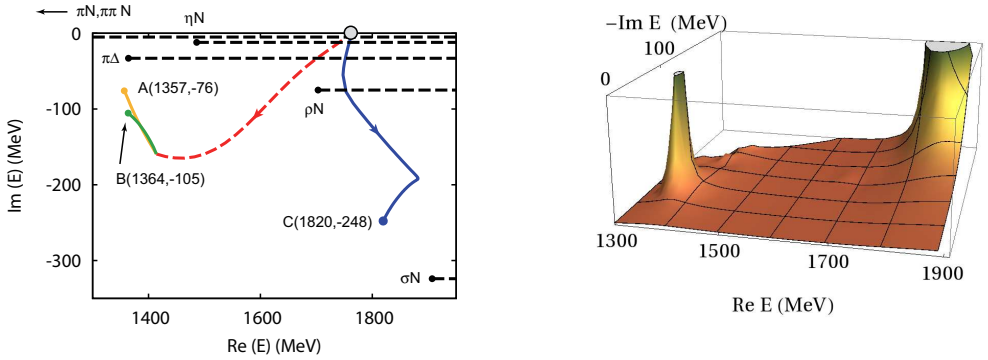

FIGURE 2. (left) Trajectories of the evolution of P_{11} resonance poles A (1357,76), B (1364,105), and C (1820,248) from a bare N^* with 1763 MeV, as the couplings of the bare N^* with the meson-baryon reaction channels are varied from zero to the full strengths of the JLMS model. See text for detailed explanations. Brunch cuts for all channels are denoted as dashed lines. The branch points, $E_{\text{b.p.}}$, for unstable channels are determined by $E_{\text{b.p.}} - E_M(k) - E_B(k) - \Sigma_{MB}(k, E_{\text{b.p.}}) = 0$ of the their propagators (described in the text) evaluated at the spectator momentum k=0. With the parameters [2] used in JLMS model, we find that $E_{\text{b.p.}}$ (MeV) $= (1365.40, -32.46), (1704.08, -74.98), (1907.57, -323.62)$ for $\pi\Delta$, ρN, and σN, respectively. (right) 3-Dimensional depiction of the behavior of $|\det[D(E)]|^2$ of the P_{11} N^* propagator (in arbitrary units) as a function of complex-E.

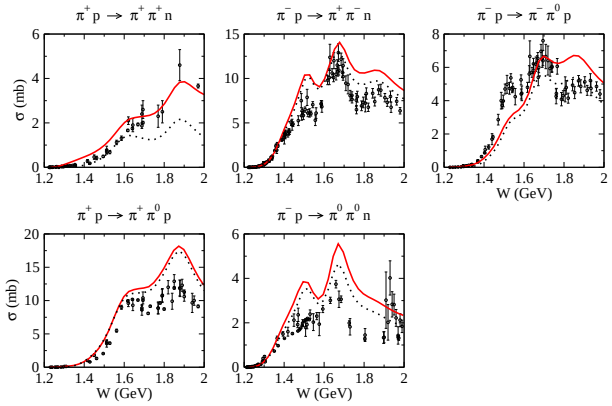

FIGURE 3. The total cross sections predicted (solid curves) from the JLMS model are compared with the experimental data. The dotted curves are from turning off the amplitude $T^{\text{dir}}_{\pi N,\pi\pi N}$. Experimental data are from Ref. [13]

In order to determine the parameters, a data set including 294 measured differential cross-sections, coming from five collaborations, were fitted. The selection of data points allows to suppress the manifestations of inconsistencies among available data sets. The best model, named B in [14], reproduces satisfactorily the data, with a reduced χ^2 = 1.94. A detailed study of the reaction mechanism within the model allows to establish a hierarchy in the roles played by nucleon resonances. Actually, the dominant resonant turns out to be the $S_{11}(1535)$. The other resonances affecting the χ^2 by more than 20% when switched off, are by decreasing importance: $P_{11}(1440)$, $P_{13}(1720)$, $S_{11}(1650)$, $F_{15}(1680)$, $P_{11}(1710)$, and $D_{13}(1520)$. Contributions from $D_{13}(1700)$ and $D_{15}(1675)$ are found to be negligible. In fig. 4 we present a comparison of the total cross section computed with our model with the data, more detailed information can be found in Ref. [14].

ELECTROMAGNETIC PRODUCTION

As outlined in the introduction, the main aim of the EBAC is to analyze the extant photo and electroproduction data, measured mainly in Germany (MAMI and Bonn) and the USA (Jefferson Lab) and settle the baryon spectrum, extracting and interpreting the properties of the nucleon resonances.

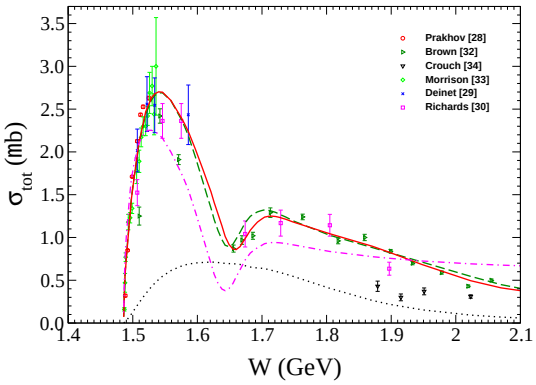

FIGURE 4. Total cross-section for the reaction $\pi^- p \to \eta n$. Curves are from Ref. [5] (dash-dotted), model *A* (dashed), model *B* (full), and the background contributions (dotted) in model *B*. Data are from [15].

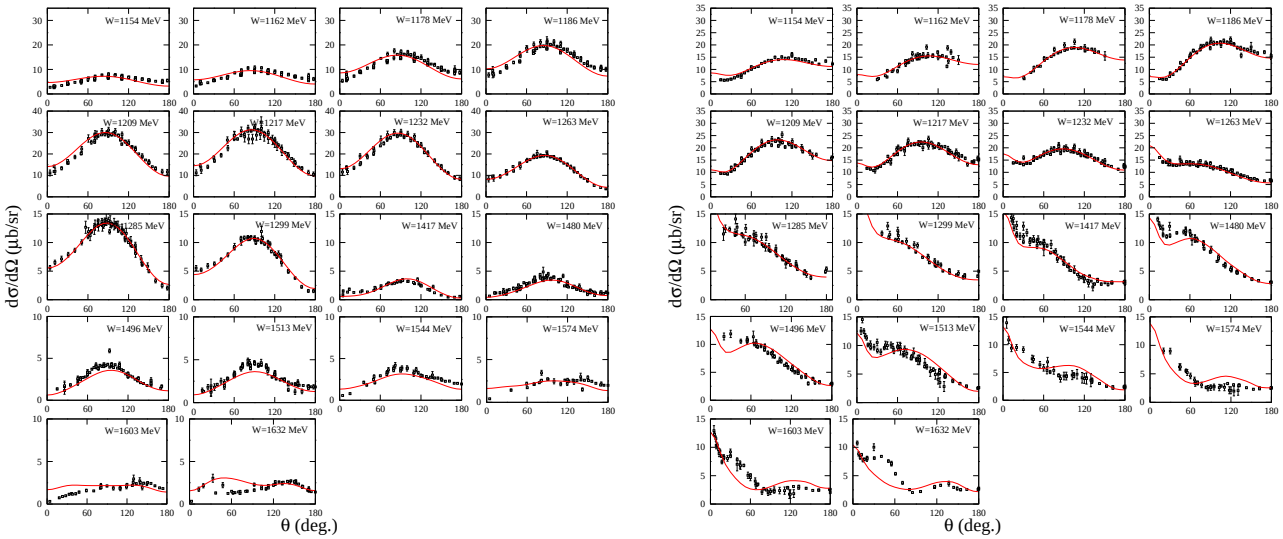

FIGURE 5. Differential cross section for $\gamma p \to \pi^0 p$ (left) and $\gamma p \to \pi^+ n$ (right) compared to experimental data obtained from Ref. [17].

Single pion photoproduction

We have applied the dynamical coupled-channels model of Ref. [2], outlined in the introduction, to investigate the pion photoproduction reactions in the first and second nucleon resonance region. With the hadronic parameters of the JLMS model of πN scattering data and the non-resonant electromagnetic couplings taken from the previous works, we showed that the available data of differential cross sections and photon asymmetries of $\gamma N \to \pi N$ up to $W = 1.65$ GeV can be described to a very large extent [16], see Fig. 5. The only free parameters in the χ^2-fit to the photoproduction data are the bare $\gamma N \to N^*$ helicity amplitudes, see Eqs. (5,6). It is found that the coupled-channels effects can have about 30 - 40 % effects in the Δ (1232) resonance region, and can drastically change the magnitudes and shapes of the cross sections in the second resonance region. We also demonstrate the importance of the loop-integrations in a dynamical approach. The meson cloud contributions to the $\gamma^* N \to N^*$ form factors have been predicted. For all cases, they are mainly in the low Q^2 region. The coupled-channels effects on the meson cloud contributions are also found to be mainly in the low Q^2 region.

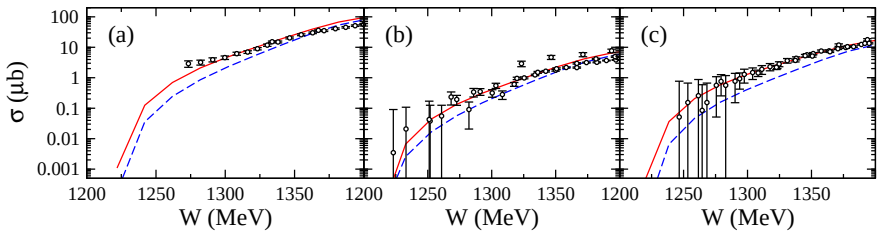

FIGURE 6. Near threshold behavior of the total cross section for $\gamma p \to \pi\pi N$: (a) $\gamma p \to \pi^+\pi^- p$, (b) $\gamma p \to \pi^0\pi^0 p$, and (c) $\gamma p \to \pi^+\pi^0 n$. The red solid curve is the full results predicted from our current model, and the blue dashed curves are the results without the $T^{\rm dir}_{\gamma N,\pi\pi N}$ contribution. The data are taken from Refs. [19].

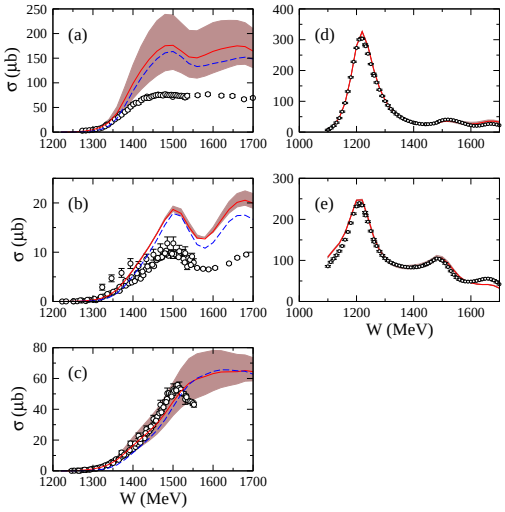

FIGURE 7. Total cross sections of the double and single pion photoproduction reactions up to $W = 1.7$ GeV: (a) $\gamma p \to \pi^+\pi^- p$, (b) $\gamma p \to \pi^0\pi^0 p$, (c) $\gamma p \to \pi^+\pi^0 n$, (d) $\gamma p \to \pi^0 p$, and (e) $\gamma p \to \pi^+ n$. The red solid curve is the full result predicted from our current model, and the blue dashed curve in (a)-(c) is the result without $T^{\rm dir}_{\gamma N,\pi\pi N}$ contribution. The band is generated by allowing a 25% variation in the value of the $\pi N\Delta$ coupling constant $g_{\pi N\Delta}$ used in the electromagnetic amplitudes. The data of the double and single pion photoproduction reactions are taken from Refs. [19] and Refs. [17], respectively.

Double pion photoproduction

We extended our single pion photoproduction model to predict the total cross sections and invariant mass distributions for two pion photoproduction reactions. The main aim is of course to be able to analyze and profit from the extensive extant data base. In Ref. [18] we preformed a detailed analysis of the current predictions from our framework. In Figs. 6 we present our prediction for the near threshold behavior of the total cross sections for three different production reactions. The predictions without any further adjusting of the parameters were not very satisfactory in the resonance region, thus we decided to explore the dependence of our predictions on some of the parameters of the model. In fig. 7 we present the effect of variations of the $\pi N\Delta$ coupling constant in the electromagnetic pieces.

Pion electroproduction reactions

The framework required for the analysis of electroproduction reactions within the dynamical coupled channels model under consideration is also described in Ref. [2]. In Ref. [20] we performed the first calculations using such framework and the hadronic pieces of the model from the JLMS model.

Electroproduction analysis have one major advantage, by varying the virtuality carried by the photon we can explore deeper into the baryon. The precise Q^2 evolution of the excitation vertexes for the different N^* states (helicity

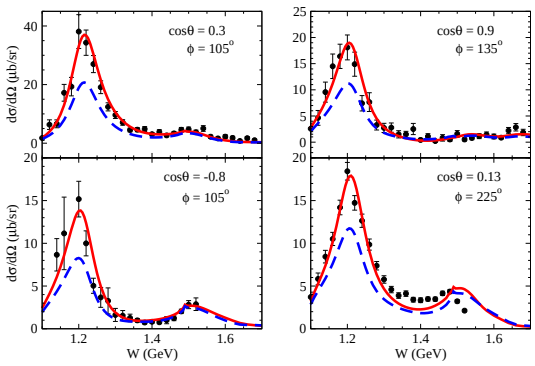

FIGURE 8. Coupled-channels effect on the five-fold differential cross sections $\Gamma_\gamma^{-1}[d\sigma^5/(dE_{e'}d\Omega_{e'}d\Omega_\pi^*)]$ of $p(e,e'\pi^0)p$ (upper panels) and $p(e,e'\pi^+)n$ (lower panels) at $Q^2 = 0.4$ (GeV/c)^2. Here $\theta \equiv \theta_\pi^*$ and $\phi \equiv \phi_\pi^*$. The solid curves are the full results calculated with the bare helicity amplitudes of Fit1. The dashed curves are the same as the solid curves but only the πN loop is taken into account, see Ref. [20] for details. The data are taken from Ref. [25]

amplitudes) is thus a subject of intensive study, see for instance Refs. [21, 22, 23].

The quantity relevant to our discussions is the dressed $\gamma^* N \to N^*$ vertex function defined by

$$\begin{aligned}\bar{\Gamma}^J_{N^*,\lambda_\gamma\lambda_N}(q,W,Q^2) &= \Gamma^J_{N^*,\lambda_\gamma\lambda_N}(q,Q^2) \\ &+ \sum_{M'B'}\sum_{L'S'}\int k'^2 dk' \bar{\Gamma}^J_{N^*,L'S'M'B'}(k',W) G_{M'B'}(k',W) v^J_{L'S'M'B',\lambda_\gamma\lambda_N}(k',q,Q^2)\,.\end{aligned} \tag{7}$$

The second term of Eq. (7) is due to the mechanism where the non-resonant electromagnetic meson production takes place before the dressed N^* states are formed. Similar to what was defined in previous works, we call this contribution the *meson cloud effect*. Let us emphasize that the meson cloud term in Eq. (7) is the necessary consequence of the unitarity conditions. How this term and the assumed bare N^* states are interpreted is obviously model dependent.

Within the one-photon exchange approximation, the differential cross sections of pion electroproduction can be written as a function of several structure functions,

$$\frac{d\sigma^5}{dE_{e'}d\Omega_{e'}d\Omega_\pi^*} = f(\sigma_T,\sigma_L,\sigma_{LT},\sigma_{TT},\sigma_{LT'}) \tag{8}$$

The formula for calculating σ_α from the amplitudes are given in Ref. [24]. In this first-stage investigation, we only considered the data of structure functions σ_α of $p(e,e'\pi^0)p$ and $p(e,e'\pi^+)n$ up to $W = 1.6$ GeV and $Q^2 = 1.45$ (GeV/c)^2.

To proceed, we need to define the bare $\gamma^* N \to N^*$ vertex functions $\Gamma^J_{N^*,\lambda_\gamma\lambda_N}(q,Q^2)$ of Eq. (7). We parameterize these functions as $\Gamma^J_{N^*,\lambda_\gamma\lambda_N}(q,Q^2) = 1/(2\pi)^{3/2}\sqrt{m_N/E_N(q)}\sqrt{q_R/|q_0|}G_\lambda(N^*,Q^2)\delta_{\lambda,(\lambda_\gamma-\lambda_N)}$, where q_R and q_0 are defined by $M_{N^*} = q_R + E_N(q_R)$ with N^* mass and $W = q_0 + E_N(q_0)$, respectively.

The only freedom in this study for analyzing the electromagnetic meson production reactions is the electromagnetic coupling parameters of the model. If the parameters listed in Ref. [2] are used to calculate the non-resonant interaction $v^J_{L'S'M'B',\lambda_\gamma\lambda_N}(k',q)$ in Eq. (7), the only parameters to be determined from the data of pion electroproduction reactions are the bare helicity amplitudes defined above.

As an example of the obtained results reported in Ref. [20] we present in Fig. 8 a sample of the five fold differential cross section together with the importance of πN intermediate loops in the electromagnetic production cross sections.

SUMMARY AND FUTURE PERSPECTIVES

Since it was initiated in 2006, the Excited Baryon Analysis Center has been playing an important role in the effort to extract and interpret nucleon resonance properties from the extant data of hadronic and electromagnetic single and

double meson production reactions. A number of publications, briefly sketched in this proceedings, have resulted which basically touch almost all of the relevant experimental data which need to be ultimately correlated within the same framework. The ability of the dynamical coupled channels model to serve as common framework to correlate hadronic and electromagnetic meson production reactions has been shown already through the several topics described in this proceedings. In the near future a major effort will be pursued to extend the description of electromagnetic reactions up to $W = 2$ GeV and $Q^2 \sim 6$ GeV^2, and to incorporate into the framework the KY channels.

ACKNOWLEDGMENTS

I would like to thank J. Durand, H. Kamano, T.-S. H. Lee, A. Matsuyama, T. Sato, B. Saghai, and N. Suzuki for the collaborations we have kept during the last years. I thank also R. Arndt, M. Doering, S. Krewald and C. Hanhart for discussions and comments on parts of this work, and the organizers of the Hadron 2009 conference for the nice meeting. This work is supported by a CPAN CSD 2007-0042 contract, and by Grant No. FIS2008-1661 (Spain). The computations were performed at NERSC (LBNL) and Barcelona Supercomputing Center (BSC/CNS) (Spain). The authors thankfully acknowledge the computer resources, technical expertise and assistance provided by the Barcelona Supercomputing Center - Centro Nacional de Supercomputacion (Spain).

REFERENCES

1. V. Burkert and T.-S. H. Lee, Int. J. of Mod. Phys. **E13**, 1035 (2004).
2. A. Matsuyama, T. Sato, and T.-S. H. Lee, Phys. Rep. **439**, 193 (2007).
3. B. Julia-Diaz, H. Kamano, T. S. Lee, A. Matsuyama, T. Sato and N. Suzuki, Chin. J. Phys. **47**, 142 (2009).
4. R. A. Arndt, W. J. Briscoe, I. I. Strakovsky, and R. L. Workman, Phys. Rev. C **74**, 045205 (2006).
5. B. Julia-Diaz, T.-S. H. Lee, A. Matsuyama, and T. Sato, Phys. Rev. C **76**, 065201 (2007).
6. N. Suzuki, T. Sato, and T.-S. H. Lee, Phys. Rev. C **79**, 025205 (2009).
7. N. Suzuki, T. Sato and T. S. Lee, arXiv:0910.1742 [nucl-th].
8. N. Suzuki, B. Julia-Diaz, H. Kamano, T.-S. H. Lee, A. Matsuyama, and T. Sato, arXiv:0909.1356 [nucl-th], to appear in Phys. Rev. Lett. (2010).
9. C. Amsler *et al.* (PDG) Phys. Lett. **B667**, 1 (2008).
10. R.E. Cutkosky, S. Wang, Phys. Rev. **D42**, 235 (1990).
11. M. Doring, *et al.*, Phys.Lett. **B 681**, 26, (2009), Nucl.Phys.A **829**, 170 (2009).
12. H. Kamano, B. Julia-Diaz, T.-S. H. Lee, A. Matsuyama, and T. Sato, Phys. Rev. C **79**, 025206 (2009).
13. G. Kernel *et al.*, Phys. Lett. **B216**, 244 (1989); G. Kernel *et al.*, Phys. Lett. **B225**, 198 (1989); J. Lowe *et al.*, Phys. Rev. C **44**, 956 (1991); S. Prakhov *et al.*, Phys. Rev. C **69**, 045202 (2004); M. E. Sevior *et al.*, Phys. Rev. Lett. **66**, 2569 (1991); D. Počanić *et al.*, Phys. Rev. Lett. **72**, 1156 (1994); G. Kernel *et al.*, Z. Phys. C **48**, 201 (1990).
14. J. Durand, B. Julia-Diaz, T.-S. H. Lee, B. Saghai, and T. Sato, Phys. Rev. C **78**, 025204 (2008).
15. T. W. Morrison, PhD Thesis, George Washington University, UMI-99-55477 (2000); S. Prakhov *et al.*, Phys. Rev. C **72**, 015203 (2005); W. Deinet *et al.*, Nucl. Phys. **B11**, 495 (1969); W. B. Richards *et al.*, Phys. Rev. D **1**, 10 (1970); N. C. Debenham *et al.*, Phys. Rev. D **12**, 2545 (1975); R. M. Brown *et al.*, Nucl. Phys. **B153**, 89 (1979); R. H. Crouch *et al.*, Phys. Rev. D **21**, 3023 (1980); J. Feltesse *et al.*, Nucl. Phys. **B93**, 242 (1975).
16. B. Julia-Diaz, T.-S. H. Lee, A. Matsuyama, T. Sato, and L. C. Smith, Phys. Rev. C **77**, 045205 (2008).
17. GWU-CNS, http://gwdac.phys.gwu.edu/
18. H. Kamano, B. Julia-Diaz, T. S. Lee, A. Matsuyama and T. Sato, Phys. Rev. C **80**, 065203 (2009).
19. ABBHHM Collaboration, Phys. Rev. **175**, 1669 (1968); A. Braghieri *et al.*, Phys. Lett. B **363**, 46 (1995); M. Wolf, *et al.*, Eur. Phys. J. A **9**, 5, (2000); W. Langgärtner, *et al.*, Phys. Rev. Lett. **87**, 052001, (2001); Y. Assafiri *et al.*, Phys. Rev. Lett. **90**, 222001 (2003); J. Ahrens *et al.* (GDH and A2 Collaborations), Phys. Lett. B **551**, 49 (2003); J. Ahrens *et al.* (GDH and A2 Collaborations), Phys. Lett. B **624**, 173 (2005).
20. B. Julia-Diaz, T.-S. H. Lee, A. Matsuyama, T. Sato, and L. C. Smith, Phys. Rev. C **80**, 025207 (2009).
21. V. Pascalutsa, M. Vanderhaeghen, S. N. Yang, Phys. Rept. **437** 125 ,(2007).
22. Huey-Wen Lin, Saul D. Cohen, Robert G. Edwards, David G. Richards Phys. Rev. D **78** 114508, (2008).
23. B. Julia-Diaz, D.O. Riska, and F. Coester, Phys. Rev. **C69**, 035212 (2004).
24. T. Sato and T.-S. H. Lee, J. Phys. G 36, 073001 (2009).
25. K. Joo et al. (CLAS), Phys. Rev. Lett. 88, 122001; H. Egiyan et al. (CLAS), Phys. Rev. C73, 025204, 2006; CLAS Physics Database, JLab (Hall B), http://clasweb.jlab.org/cgi-bin/clasdb/db.cgi .